Insights into the Electronic Dynamics in Chemical Reactions

Daniel Aktah, Daniele Passerone,*,† and Michele Parrinello‡

CSCS−Swiss Center for Scientific Computing, Via Cantonale, 6928 Manno, Switzerland, and Department of Physical Chemistry, Swiss Federal Institute of Technology (ETH), Hönggerberg HCI, 8093 Zurich, Switzerland

Received: August 29, 2003

We study with an ab initio molecular dynamics method the bond-breaking and bond-forming processes in chemical reactions. To obtain reactive trajectories, we use a newly developed method based on the optimization of a suitably defined action. The Hellmann−Feynman forces, which are needed to optimize the action, are calculated within density-functional theory. We contrast a concerted [4+2] cycloaddition of cyclopentadiene and ethylene with the nonconcerted [2+2] cycloaddition of two ethylene molecules. We find that the duration of the bond-breaking and bond-forming processes due to the nuclear motion is ∼100 fs. Moreover the electronic delocalization, as well as the HOMO−LUMO energy gap during the two reactions, allows us to distinguish clearly between the concerted and the nonconcerted mechanism.

Introduction

With each chemical reaction is associated a characteristic time scale determined by the height of the transition state barrier. Most of this time is spent waiting for the fluctuation that is able to bring the system across the energy barrier separating reactants from products. The actual crossing time is much shorter and for many reactions can be estimated as being on the order of picoseconds. During this time, a massive rearrangement of bonds takes place, such as the one depicted in Scheme 1. The questions that we wish to address here are how does this crucial step take place, how long does it last, and can it be measured? In other words, is it instantaneous, as is implicitly assumed, or has it a finite duration and its own measurable dynamics? A positive answer to these latter questions will have a bearing on our understanding of chemical reactions and provide a tool to determine the reaction mechanism in an unambiguous fashion.

To study the dynamics of the bond-breaking and bond-forming processes and answer these questions, we use a novel method[1,2] that allows approximate dynamical trajectories with preassigned initial ("*A*") and final positions ("*B*") to be computed. We underline that this is at variance with ordinary quantum chemical methods in high dimensions, where the study of the real dynamics is neglected and only the intrinsic reaction coordinate is computed.[3,4] It was recently shown that this can lead to the prediction of incorrect transition states, and one could easily draw spurious conclusions regarding the mechanism of transitions between the reactants $\mathscr{A}$ and the products $\mathscr{B}$.[5] To be specific, we study two prototypical thermal cycloadditions (Scheme 1). The first is the Diels−Alder reaction of ethylene and cyclopentadiene leading to the formation of norbornene (eq 1). The second is the [2+2] cycloaddition of two ethylene molecules (eq 2).

Given their relevance very many theoretical and experimental investigations have been carried out to understand and explore this class of chemical reactions.[6−30] Recent femtosecond-resolved experiments by Horn, Herek, and Zewail have studied the retro-Diels−Alder reaction of norbornene[15,16] and proposed concerted, as well as nonconcerted, reaction mechanisms under the pump−probe reaction conditions. More recently, Fuss and collaborators[17] showed that excited-state norbornene undergoes bond cleavage leading to ground-state carbenes rather than retro-Diels−Alder products. The authors concluded that cyclopentadiene is most probably the result of a "hot" ground-state reaction. Gas-phase static reactor studies on deuterium-substituted norbornene however have shown that norbornene fragments under stereochemical retention within the current detection limits.[18] Therefore no definite conclusion can be reached. Static calculations of Houk and collaborators based on density-functional theory at the B3LYP/6-31G* and the CASSCF/6-31G* level showed that the concerted pathway is the lowest energy path on the ground-state surface.[19,20] In contrast, in the [2+2] cycloaddition, experimental data showed that the gas-phase cycloaddition of ethylene to (*E*)- and (*Z*)-but-2-ene is not stereospecific.[21,22] Static calculations predict a nonconcerted, stepwise pathway over a biradicaloid intermediate and emphasize the flatness of the energy landscape in that region.[26−29]

SCHEME 1

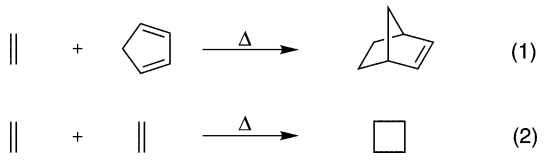

Despite this evidence, an issue that is much debated in these as well as in other reactions is whether the mechanism is concerted, that is, whether the bonds of the ring system are formed in one or several steps, via the formation of an intermediate species, which can be a biradicaloid or a zwitterion. So far, the mechanism has been decided on the basis of experimentally observed stereospecificity. However, high stereospecificity alone cannot be sufficient.[31] In fact, if in a nonconcerted reaction the cyclization is faster than the competing isomerization of the intermediate, the final product could be the same as in the concerted process. In the following on

* To whom correspondence should be addressed. E-mail: dpassero@inf.ethz.ch.

† Present address: Computational Laboratory (COLAB), Swiss Federal Institute of Technology (ETH), Hirschengraben 84, 8092 Zurich, Switzerland.

‡ Present address: Computational Science, Department of Chemistry and Applied Biosciences ETH Zurich, USI-Campus, Via Giuseppe Buffi 13, 6900 Lugano, Switzerland.

10.1021/jp036572y CCC: $27.50
Published on Web 01/13/2004

the basis of our theoretical studies, we shall propose experiments that could unambiguously discriminate between the two possibilities.

Computational Methods

If the energy barrier between reactants $\mathscr{A}$ and product $\mathscr{B}$ is high, the spontaneous observation of a reaction event during a conventional ab initio molecular dynamics is very unlikely. For this reason, we use a recently developed method,[1,2] which allows rare events to be studied.

Conventional molecular dynamics (MD) methods are not the appropriate choice for studying processes (such as a chemical reaction) where reactants and products are separated by one (or more than one) high free energy barrier. Indeed, if the system is prepared in the basin of the reactants with certain initial conditions in its positions and velocities, its evolution, as determined by an algorithm of integration of the equations of motion, will leave the system in the same basin for a very long time. This is because the probability of crossing the barrier decays exponentially with the barrier height. On the other hand, since the initial and the final state of the reaction are known, and the actual barrier crossing is usually a fast event in itself, it is possible in some cases to switch from an initial value formulation (relying on the time discretization of the equations of motion) to a two-point boundary variational formulation, relying on the variational principles of classical mechanics. Also in the so-called ab initio MD such as Born−Oppenheimer (BO) or Car−Parrinello MD, the equations of motion are derived from a Lagrangian (the difference between *T*, the kinetic energy, and *V*, the potential energy, of the system), whose time integral along the trajectory (the action) is *stationary* for physical paths connecting two points in the configuration space. More precisely, Hamilton's principle states that every physical trajectory connecting two points *A* and *B* in configuration space renders the action integral, $S_H = \int_0^\tau (T(\dot{\vec{q}}(t)) - V(\vec{q})(t)))dt$, stationary with respect to variations in the path (the total time of the trajectory is kept fixed). The inputs of our method are therefore the initial configuration in "*A*" (reactants), the final configuration in "*B*" (product), and the total time τ. In our methodology, the integral is transformed into a finite sum and the trajectory connecting *A* and *B* is a sort of "polymer" composed by $P = \tau/\Delta$ beads, where Δ is a suitably chosen time step. Since the stationary point of S_H is in most cases not a minimum but a saddle point, our method introduces a modified action $S_\Theta = S_H + \mu \int_0^\tau (E(t) - \bar{E})^2 \, dt$, where the additional term is a penalty function enforcing the conservation of energy. The minimum of S_Θ is found with respect to the Fourier components of the trajectory, which is treated as a band drawn from *A* to *B*. As discussed in refs 1 and 2, the minimum of this action is not necessarily coincident with the stationary point of S_H. It is nevertheless an energy conserving trajectory (at variance with the so-called minimum energy path (MEP), where all fast oscillations are damped; the MEP can be obtained with a variety of methods such as the nudged elastic band method[32] and the string method[33]), which represents a good approximation to a solution of the original variational problem. This is true in particular in the most interesting transition region. It is in the latter sense that we will refer in this paper to a minimum of an S_Θ functional as an "approximate dynamical trajectory" (or Θ-trajectory). Starting from S_Θ, a further optimization could be performed (leading to more precise trajectories, solutions of the original variational problem) as described in ref 2. In the particular case of the systems discussed in this paper, we had already caught the interesting features of the trajectories with the minimization of the S_Θ, and we did not push the optimization further.

In this framework, it is clear that "*A*" and "*B*" are fully interchangeable, so that both the reaction path and its retro path are obtained from this procedure, due to the principle of microscopic reversibility. The potential energies and forces along the path are calculated within the framework of density-functional theory. An important advantage of the method is that it only requires the calculation of the Hellmann−Feynman forces and that it can be trivially parallelized. The trajectory is suitably parametrized and the action is minimized relative to these parameters.[2] We calculate the forces at each time step by finding the electronic ground state and using the Hellmann−Feynman theorem. The implementation of the method is based on an interface, which combines the minimization of the action (Vergilius code[2]) with the ab initio calculation of the potential energies and forces on the nuclei (CPMD[34] and Gaussian 98 code[35]) using a parallel architecture. We used Kohn−Sham theory in the local-spin density approximation and the BLYP density functional.[36−40] In addition, for the [2+2] cycloaddition the hybrid density functional B3LYP was also used.[41] While BLYP was used in the CPMD-code, for the hybrid functional B3LYP[41] the Gaussian 98 program was utilized.

Within the CPMD code periodic boundary conditions were employed and the wave functions were represented by plane waves with a certain plane-wave cutoff. To reduce the computational cost of the calculation, we started the minimization with a relatively small plane-wave energy cutoff of $E_c = 20$ Ry, and used a small cubic supercell with edge $L \simeq 7.41$ Å. For this cutoff, the pseudopotentials of Martins and Troullier[42] have been used for describing the core electrons. Though not sufficiently accurate, this approach allowed us to obtain a first trajectory containing already most of the relevant information concerning the reaction mechanism. Then, the accuracy of the calculation was systematically increased, and we compared the energy profile to all-electron calculations. We observed that by increasing the cutoff to $E_c = 40$ Ry and using the pseudopotentials of Goedecker, Teter, and Hutter,[43] the energy profile agreed well with all-electron calculations using a standard 6-31G(d) basis set. Therefore the minimization was continued with a cutoff of $E_c = 40$ Ry. In a final step, the accuracy was further increased by using a cutoff of $E_c = 70$ Ry and a cubic simulation box with edge $L \simeq 10.58$ Å. These are the values that have been found to give converged energy differences with respect to very large plane-wave cutoffs and total energies that are converged with respect to the volume of the supercell.

Within the Gaussian 98 code, on the other hand, a standard 6-311++G(d,p) basis set was used. We found that in the case of the [2+2] cycloaddition, larger basis sets including the augmented correlation-consistent basis set, aug-cc-pVQZ, lead to energy differences of only 1 kcal/mol. To destroy the $\alpha-\beta$ and spatial symmetries in the initial guess wave functions, the HOMO and LUMO were mixed. Furthermore, a tighter SCF convergence criterion was chosen.

Within the Vergilius code, we used a preconditioned conjugated gradient algorithm to minimize the action. To enforce total energy conservation, we used a μ value in the range between $\mu_{min} = 10^4$ and $\mu_{max} = 10^6$.[1] The total time τ was chosen on the basis of available experience with simpler systems:[1] if the total time is too small, the minimization of the $\mathscr{S}_\theta$-functional at a given energy *E* is problematic. On the other hand, if τ is too long the system simply stays longer in one or both basins of attraction; but this does not affect the true reaction time. Therefore if τ is sufficiently large, its precise value is not crucial. In this case, we divided the trajectories into 144 and 130 steps for a total time of ∼349 and ∼315 fs for the [4+2] and the

[2+2] cycloaddition, respectively. As starting trajectories, we used a linear interpolation between the initial and final positions. In addition, we randomized the coordinates to introduce vibrational disorder from the start. By decreasing the total energy of the system, we lowered systematically the potential-energy barrier of the path.

To visualize the electronic motion, we use the centroids of Boys localized orbitals.[44] The Boys orbitals are obtained by the unitary transformation of the Kohn−Sham orbitals, which minimize the mean quadratic spread, $\Omega = \sum_{i=1}^{N\,state} \langle r_i^2 \rangle - \langle r_i \rangle^2$.[45−47] They are the nonperiodic version of the Wannier orbitals, and for the latter, it has been shown that the centroid's motion current gives the real electronic current.[48] In practice, since we use periodic boundary conditions, the Boys centers are calculated as if they were Wannier-function centers. The corresponding spread functional that we have used is the one of Silvestrelli.[46,47]

Results and Discussion

A. Dynamical Study of the [4+2] Cycloaddition of Ethylene and Cyclopentadiene. We start with the discussion of the Diels−Alder reaction of ethylene and cyclopentadiene. From the dynamical trajectory, a transition barrier of ∼25.8 kcal/mol can be estimated, which compares well with the experimental activation energy of ∼23.7 kcal/mol.[8] In selected points of this trajectory, we recalculated the energy using the Gaussian 98 program with a standard 6-311++G(d,p) basis set and the density functionals BLYP and B3LYP.[35] We find that the energy barrier estimated with B3LYP differs by 0.6 kcal/mol from the BLYP value.

Now we turn to the discussion of the trajectory. In the initial configuration A ($t = 0.0$ fs), the distance between ethylene and cyclopentadiene is $d > 3$ Å, close to 2 times the van der Waals radius of a carbon atom ($r_{VdW}(C) = 1.7$ Å[49]). It should be noticed that the relative orientation was set randomly in order not to bias the path optimization. The final configuration B is given by the norbornene molecule. Four characteristic configurations along a trajectory obtained from the $\mathcal{J}_\theta$-minimization are depicted in Figure 1. During the reaction process the two molecules, ethylene and cyclopentadiene, approach each other, and the initial asymmetry decreases. At $t = 261.4$ fs, the configuration of the system is very symmetric. Then the intercarbon distances decrease further until B has formed ($t =$ 348.5 fs).

To analyze the reaction mechanism, we monitored the C^1-C^4 and the C^2-C^3 bond distances along the path (Figure 2a). During the reaction process, the distances decrease and approach each other. After $t \simeq 200$ fs, both distances decrease almost simultaneously until norbornene has formed. The reaction mechanism is therefore concerted in agreement with the picture that emerges from static calculations.[19]

The rearrangement of covalent bonds can be nicely followed in time by monitoring the distances of the original π-bonds and the σ-bond, which is transformed into a π-bond in the product molecule norbornene (Figure 2b). For $\Delta t \simeq 200$ fs, these bond distances oscillate about their equilibrium values. Then, within about 100 fs, the distances corresponding to the double bonds increase, while the distance corresponding to the single bond decreases. This collective movement of the atoms is in agreement with the concerted reaction mechanism. But, more interestingly, the duration of the bond-breaking and bond-forming process due to the motion of the nuclei is about 100 fs. Furthermore, there are two characteristic bond distances describing the transition-state region: One is given by the crossing point of the distance curves (Figure 2b), that is, at $t \simeq$ 259 fs, and is about 1.4 Å; note that this distance is close to the C−C bond distance of the benzene molecule. The other one is determined by the carbon−carbon bond-forming distances, C^1-C^4 and C^2-C^3 (Figure 2a) and is at this time in the range between 2.2 and 2.3 Å.

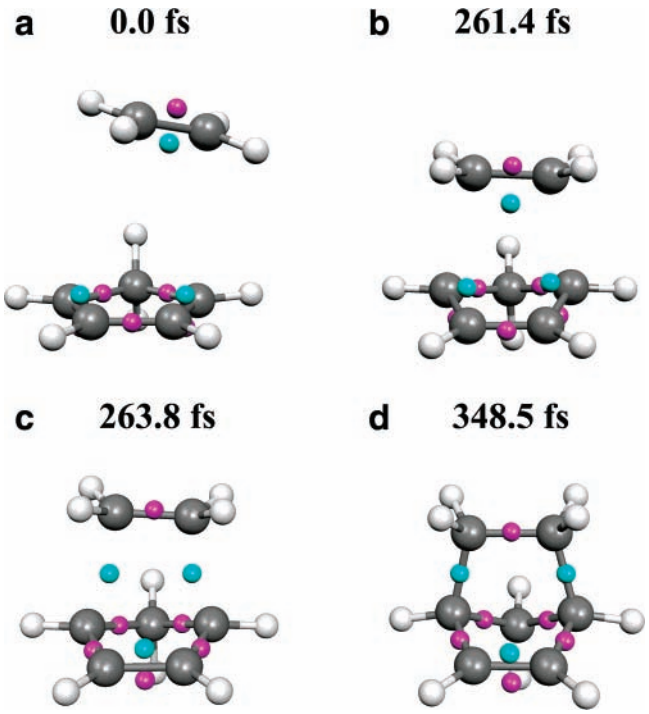

Figure 1. Four characteristic snapshots along the dynamical trajectory of the [4+2] cycloaddition of ethylene and cyclopentadiene. The carbon atoms are indicated by gray spheres, while the hydrogen atoms are represented by white spheres. In addition to the atoms, the Boys centroids of the localized wave functions are shown by smaller spheres in magenta. To emphasize their motion, six relevant reorganizing centroids are shown by cyan spheres. Note that each sphere represents two electronic centroids for α- and β-spin. Panel a shows the starting geometry of the system (0.0 fs). Panel b shows the symmetric approach of both molecules, ethylene and cyclopentadiene (261.4 fs). Note that the centroids of the electronic charge are more delocalized but their structure is still similar to the reactants. In panel c, the six relevant electronic centroids are reorganized (263.8 fs). Panel d shows the final geometry of the system (348.5 fs).

Since our reaction path should represent an approximation to the real dynamical trajectory (as could be obtained for example via the discretized Newton equations of motion using a Verlet algorithm), we analyzed further the quality of our trajectory. One possibility is to see whether our path contains a configuration of the transition-state region. A transition state in the dynamical sense should lead to reactants and products when performing a dynamics with almost no initial kinetic energy forward and backward in time. To this purpose, we ran a short Born−Oppenheimer trajectory that starts from the configuration at $t = 261.4$ fs. We initialized the velocities ($T_{init} = 1$ K) in a random manner with a tiny amount of kinetic energy and propagated the trajectory forward and backward in time in a Born−Oppenheimer fashion with $\Delta t = 0.0242$ fs. From the thus-generated trajectory, we chose the configuration at $t \simeq 199$ fs, in which both forming carbon−carbon distances are almost equal, and performed again a direct molecular dynamics run forward and backward in time ($T_{init} = 20$ K). The resulting trajectories connected basins $\mathcal{A}$ and $\mathcal{B}$, and these dynamical trajectories in the transition region had properties similar to the $\mathcal{J}_\theta$ derived one.

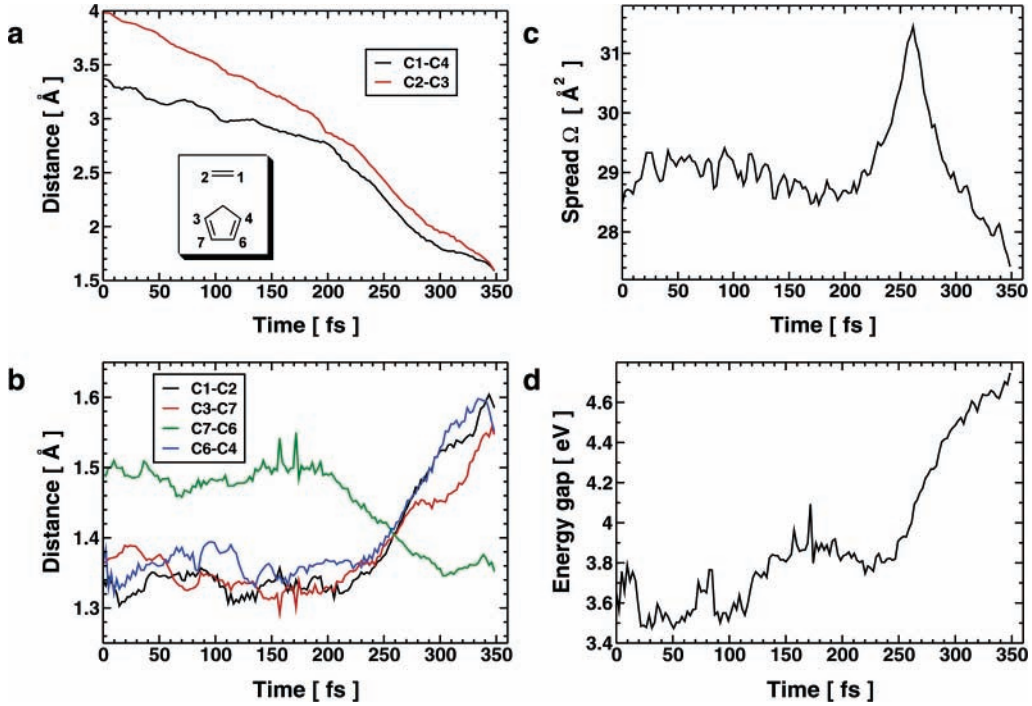

Figure 2. Bond distances, d (Å), electronic delocalization, Ω (Å^2), and the HOMO−LUMO energy gap, ΔE (eV), plotted along the reaction path: (a) the two carbon−carbon bond forming distances, C^1-C^4 and C^2-C^3, along the Diels−Alder trajectory; (b) the C^1-C^2, C^3-C,^{7} C^7-C,^{6} and the C^6-C^4 bond distances along the trajectory, describing the interconversion between π- and σ-bonds during the reaction process; (c) the total electronic spatial extent of the localized wave functions, describing the delocalization of the total electronic system along the path; (d) the HOMO−LUMO energy gap along the trajectory.

To monitor the electronic changes during the reaction process, we calculated the variation of the minimum spread functional, Ω, which describes the spatial delocalization of the electrons. As can be seen from Figure 2c, Ω is small in the initial and final configurations but changes rather abruptly on the time scale of ∼100 fs, in strong correlation with the changes in the C^1-C^4 and C^2-C^3 bond distances (see Figure 2a). We take this interval as a duration of the bond-breaking and bond-forming process. Note that the delocalization in the product is smaller than that in the reactants due to the disappearance of the two conjugated π-bonds.

Use of the Boys centroids has proven to be rather useful in the past to follow chemical processes.[50−52] In this particular case however, they proved of limited value. In fact, in the transition region, Ω is very flat with several degenerate minima, and the Boys center position is a strong function of the optimization procedure. We take this as a manifestation of aromaticity, similar to what is found in benzene when Ω has two degenerate minima corresponding to the two Kekulé structures.

To relate the observed reaction mechanism to the experiment, we calculated the HOMO−LUMO energy gap along the path. As can be seen from Figure 2d, after $\Delta t \simeq 200$ fs, the gap is characterized by a systematic increase until the product, norbornene, has formed. This increase clearly marks the concerted bond formations during the reaction and is in agreement with the change in π-bonding; cyclopentadiene has two conjugated π-bonds and should therefore have a longer absorption wavelength than the strained ring system of norbornene with only one double bond.

B. Dynamical Study of the Thermal [2+2] Cycloaddition of Two Ethylene Molecules. We now turn to the discussion of the [2+2] cycloaddition of two ethylene molecules. First we discuss the energy barrier of the reaction and the effect of the inclusion of all electrons, the basis set size, the hybrid density functional B3LYP, and dynamic correlation.

TABLE 1: Energy Differences among Three Different Configurations along the CPMD Path, Two Separated Ethylene Molecules ($t = 0$ fs), Two Approaching Ethylene Molecules ($t \simeq 70.2$ fs), and the Tetramethylene Biradicaloid ($t \simeq 213$ fs)

basis set	ΔE(213−0) [kcal/mol]	ΔE(70.2−0) [kcal/mol]
Gaussian 98		
6-311++G(d,p)	50.26	34.66
6-311++G(3df,3pd)	51.35	34.55
aug-cc-pVTZ	51.53	34.56
aug-cc-pVQZ	51.39	34.55
CPMD		
70 Ry	47.10	35.17
401 Ry	47.13	34.63

The transition barrier of the reaction path is 48 kcal/mol and has been estimated by taking the energy difference between the maximum point along the trajectory and the energies for the individual components, the two ethylene molecules ($E_{\text{Barrier}} = E_{\text{max}} - 2E_{\text{Ethylen}}$).

For specific points along the path, we recalculated the energies using the all-electron program Gaussian 98 with different basis set sizes ranging from the standard 6-311++G(d,p) basis set to the augmented Dunning basis set, aug-cc-pVQZ. As can be seen in Table 1 with use of the largest basis set aug-cc-pVQZ, the energy difference between a biradicaloid geometry ($t \simeq 213$ fs) and the reactant state A ($t = 0$ fs) is ∼51.4 kcal/mol, while the CPMD result is ∼47.1 kcal/mol for a very large plane-wave cutoff $E_c = 401$ Ry. In contrast for a nonbiradicaloid system like the configuration at $t \simeq 70.2$ fs, a very good agreement between CPMD and Gaussian 98 in the energy differences with respect to the reactant configuration A is observed. This energetic deviation in the biradicaloid region is probably due to the pseudopotential.

To eliminate this source of error, we optimized $\int_\theta$ using the interface to the Gaussian 98 program starting from the CPMD

TABLE 2: The Energy Difference between Two Relevant Configurations (the Geometries at $t = 0$ and 217.8 fs) along the Refined BLYP Trajectory[53]

method	$\Delta E(217.8-0)$ [kcal/mol]
UBLYP	50.676
UB3LYP	46.618
UMP2(FC)	45.102
UMP2(FULL)	44.975
UMP4(FC)	44.923

trajectory. For the calculations, the standard 6-311++G(d,p) basis set and the BLYP density functional were used. The transition barrier obtained is now ~51.8 kcal/mol and is still larger than the experimental activation energy (~44 kcal/mol[9]). The trajectory did not change much with respect to the CPMD path, which is indicated by the small Euclidean distance between the two trajectories ($D \simeq 3 \times 10^{-3}$ Å/atom/slice).

For estimating the influence of explicit Hartree−Fock exchange and dynamic correlation on the reaction barrier, the energy difference between two relevant configurations along the previous reaction path was determined. As can be seen from Table 2, the hybrid density functional B3LYP decreases the energy difference by about 4 kcal/mol. The inclusion of dynamic correlation by using MP2 and MP4 further decreased the barrier only slightly (~1.7 kcal/mol).

Eventually, we refined the reaction path further by minimizing the $\mathcal{J}_\theta$-action and using the B3LYP density functional. The final transition barrier estimated from the reaction path is now ~47.3 kcal/mol, agreeing well with the experimental activation energy (~44 kcal/mol[9]). Moreover, the energy gap along the trajectory is almost constantly shifted toward larger values by about 2 eV, maintaining the qualitative picture reflected by the BLYP profile.

We turn now to the discussion of the trajectory. In the initial configuration *A* ($t = 0$ fs), both ethylene molecules are well separated from each other by a distance larger than 4 Å, which is over 2 times the van der Waals radius of a carbon atom ($r_{vdW}(C) = 1.7$ Å[49]). The final configuration *B* is given by cyclobutane with its characteristic butterfly structure. As in the [4+2] cycloaddition, the relative orientation of the two ethylene molecules is chosen randomly. Four characteristic configurations along a trajectory obtained from the $\mathcal{J}_\theta$-minimization are depicted in Figure 3. During the reaction process, the C^1-C^4 bond is formed first ($t \simeq 184$ fs). This configuration has a dihedral angle of $\phi = 67°$, which is close to a gauche conformation. After the system undergoes a dihedral rotation and passes through the perfect gauche conformer, $\phi = 60°$, it tends to close the ring until cyclobutane is formed ($t \simeq 315$ fs).

This stepwise mechanism can be seen in Figure 4a, where we plot the carbon−carbon bond-forming distances, C^1-C^4 and C^2-C^3, along the path. This indicates a nonconcerted reaction mechanism, in agreement with the picture emerging from static calculations.[26]

Similarly to what was done for the [4+2] cycloaddition reaction, we monitor the electronic changes during the reaction process by observing the variation of the minimum spread functional, Ω. In agreement with the stepwise formation of covalent bonds, two maxima in the electronic delocalization can be recognized (Figure 4b). The time gap between these maxima is $\Delta t \simeq 100$ fs and is the lifetime of the tetramethylene biradicaloid in this particular path. As measured by the change in Ω, we find that each bond formation takes place in about 100 fs.

Contrary to the [4+2] case, here we have no problem in determining unambigiously the Boys centroids along all of the

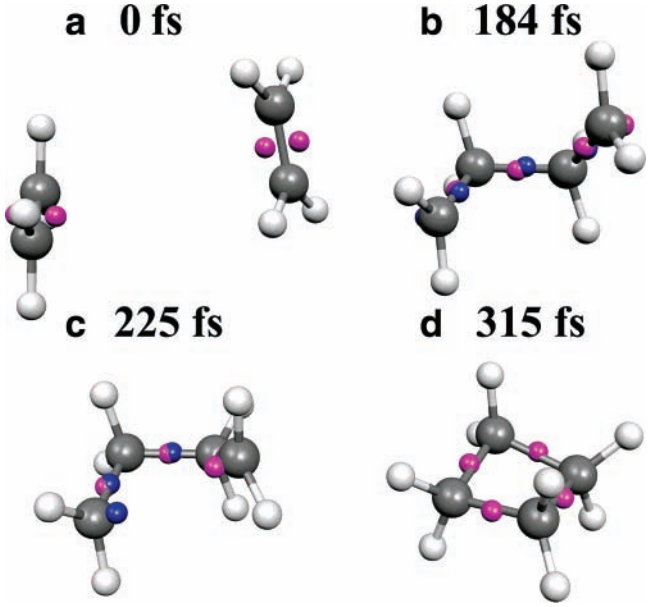

Figure 3. Four characteristic snapshots along the nonconcerted [2+2] trajectory. The valence electronic centroids of the carbon−carbon bonds are depicted with different colors (blue and magenta) for α- and β-spin. Panel a shows the starting geometry of the system (0 fs). Panel b shows the formation of the tetramethylene biradicaloid (184 fs). One carbon−carbon bond has formed, and the remaining two electronic centroids are located behind the terminal carbon atoms. Panel c shows the configuration after carbon−carbon bond rotation (225 fs). Note that here both electronic centroids have penetrated their corresponding carbon atoms for performing the final ring cyclization. Panel d shows the final geometry of the system (315 fs).

points in the path. This reflects a nonaromatic behavior along the path. Since the motion of the Boys centroids has been related to the electronic contribution to the current,[48] we plot in Figure 4c the absolute value of the velocity of four relevant Boys centroids (Scheme 2). It is seen that this quantity exhibits two large peaks separated by ~100 fs and a smaller one in between. The two larger peaks, which last ≤20 fs, correspond to the most dramatic part of the two bond-breaking and bond-forming processes. The third one reflects the transition from the biradicaloid state (Figure 3b) to the more cyclic configuration (Figure 3c). During this process, the Boys centroids of the end atoms follow the external carbons in their movement toward the formation of the new bond. The possible appearance of electronic currents opens the intriguing, albeit somewhat futuristic, possibility of directly observing these currents using nonlinear femtosecond-resolved spectroscopy.[54,55]

More simply one could measure the HOMO−LUMO energy gap (Figure 4d), which also appears different from the concerted Diels−Alder reaction of ethylene and cyclopentadiene. The reaction starts with a decrease in the energy gap from ~5.4 to ~2 eV. This is consistent with the formation of a biradicaloid, which usually has a larger absorption wavelength. After about ~150 fs, a bending is observed, indicating the formation of the first covalent bond. Then, the energy gap increases slightly reflecting the close vicinity of the two radicals. After $\Delta t \simeq 250$ fs, another bending occurs, indicating the formation of the second covalent bond. Then, the electronic system starts to relax and the energy gap increases till the end of the trajectory.

From this profile, it is evident that the energy gap is very sensitive to electronic changes in the molecular system. Not only does it provide the precise locations in time of the individual bond-breaking and bond-forming processes, but it also enables the lifetime of the biradicaloid during the reaction

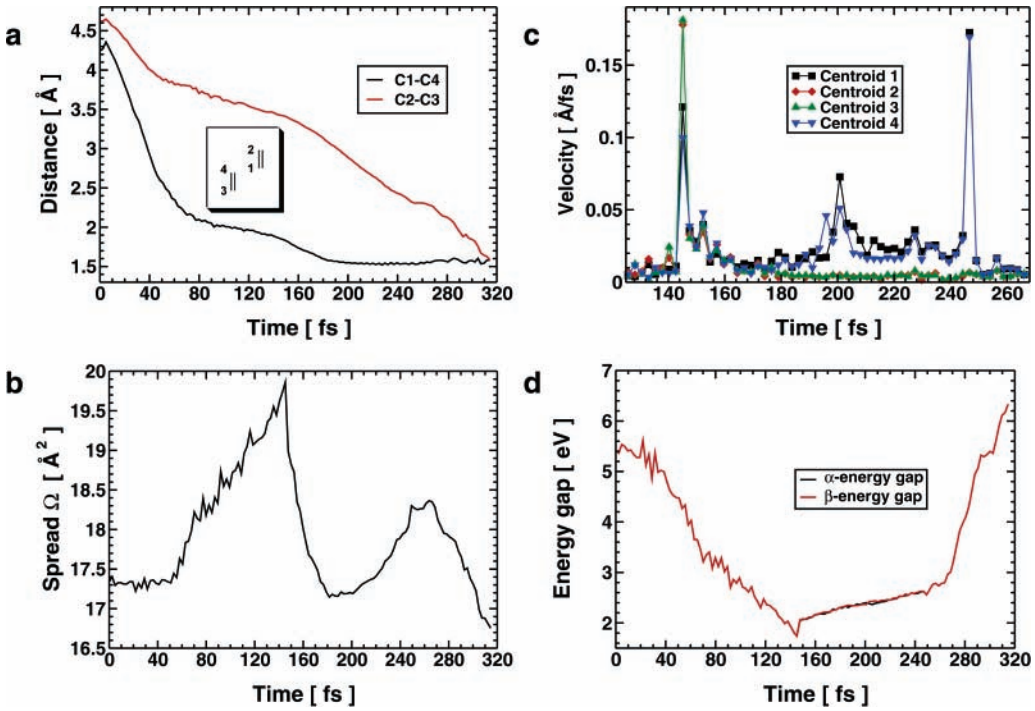

Figure 4. Bond distances, d (Å), electronic delocalization, Ω (Å^2), velocities of Boys centroids, v_{el} (Å/fs), and HOMO−LUMO energy gap, ΔE_σ, for α- and β-spin states (eV): (a) the carbon−carbon bond-forming distances C^1-C^4 and C^2-C^3 along the reaction path; (b) the total electronic spatial extent of the localized wave functions, the two maxima indicating the increased delocalization during the consecutive bond-forming and bond-breaking processes; (c) electronic velocities of four relevant centroids (see Scheme 2) zoomed into the region of the two carbon−carbon bond formations, the pattern characterizing the dynamical reorganization process of the electronic centroids during the reaction; (d) the HOMO−LUMO energy gap along the trajectory.

SCHEME 2: The Reorganization Mechanism and Numbering of the Four Boys Centroids for Which the Velocities Have Been Calculated (See also Figure 4c)

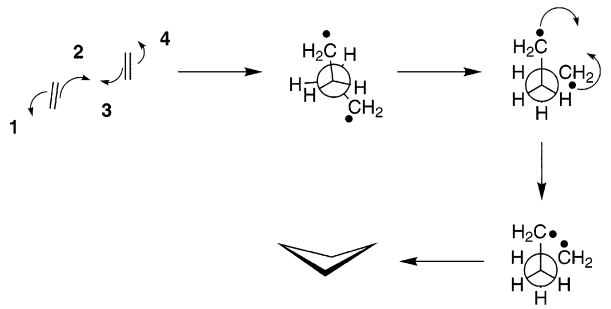

to be estimated. This time is in agreement with the ones determined by the profiles of the electronic delocalization and the electronic currents, that is, ∼100 fs.

Conclusions

We observed various relevant time scales during chemical reactions. The first one is the duration of the bond-breaking and bond-forming process due to the motion of the nuclei. We found that the transformation of a π- into a σ-bond occurs in roughly 100 fs, while the time necessary for the electrons to reorganize was found to be ≤20 fs in the case of the [2+2] cycloaddition. This is a time scale that falls within the resolution of modern femtosecond-resolved spectroscopy. For the [4+2] cycloaddition, on the other hand, no time scale due to the reorganization of the electronic centroids could be determined from the observation of the Boys centroids along the path. We mentioned that this can be explained by the flat nature of the electronic spread functional, reflecting an aromatic behavior of the transition state.

Moreover, we have shown that the change in the electronic delocalization and the HOMO−LUMO energy gap during the reactions provides a clear tool to discriminate between the concerted and the nonconcerted reaction mechanism. The individual bond formations and the lifetime of the intermediate can be clearly resolved. Thus one could imagine repeating the pump−probe experiment of Horn, Herek, and Zewail[15] on the retro Diels−Alder reaction, where one starts from norbornene and probes the "energy gap" by means of UV spectroscopy instead of mass spectrometry. Furthermore, it should be mentioned that by use of pump−probe X-ray spectroscopy, as discussed in refs 54 and 55 it is possible to measure electronic current density correlation functions, which are strongly enhanced if an electronic current flows.

We hope that our novel look at chemical bond-breaking and bond-formation processes may lead to further theoretical and experimental investigation.

Acknowledgment. D. Aktah thanks the Fonds der Chemischen Industrie and the Bundesministerium für Bildung und Forschung (BMBF) for his Kekulé scholarship. We are indebted to S. Mukamel for interesting discussions. We are grateful to J. Favre for preparing the movie of the [2+2] cycloaddition.

Supporting Information Available: Cartesian coordinates of the reactants, *A*, and the products, *B*, for the [4+2] and the [2+2] cycloaddition, Cartesian coordinates and energetics of the structures of the single-point calculations, and for the [2+2] trajectory, a movie in which the motion of the atoms and the Boys centroids can be followed (AVI format). This material is available free of charge via the Internet at http://pubs.acs.org.

References and Notes

(1) Passerone, D.; Parrinello, M. *Phys. Rev. Lett.* **2001**, *87*, 108302-1−108302-4; **2003**, *90*, 089802-1.

(2) Passerone, D.; Ceccarelli, M.; Parrinello, M. *J. Chem. Phys.* **2003**, *118*, 2025−2032.
(3) Fukui, K. *Science* **1982**, *218*, 747−754.
(4) Gonzalez, C.; Schlegel, H. B. *J. Chem. Phys.* **1989**, *90*, 2154−2161.
(5) Ammal, S. C.; Yamataka, H.; Aida, M.; Dupuis, M. *Science* **2003**, *299*, 1555−1557.
(6) Woodward, R. B.; Hoffmann, R. *Angew. Chem., Int. Ed. Engl.* **1969**, *8*, 781−853.
(7) Sauer, J.; Sustmann, R. *Angew. Chem.* **1980**, *92*, 773−801.
(8) Walsh, R.; Wells, J. M. *J. Chem. Soc., Perkin Trans.* **1976**, *2*, 52−55.
(9) Quick, L. M.; Knecht, D. A.; Back, M. H. *Int. J. Chem. Kinet.* **1972**, *4*, 61−68.
(10) Houk, K. N.; Li, Y.; Evanseck, J. D. *Angew. Chem., Int. Ed. Engl.* **1992**, *31*, 682−708.
(11) Houk, K. N.; González, J.; Li, Y. *Acc. Chem. Res.* **1995**, *28*, 81−90.
(12) Isobe, H.; Takano, Y.; Kitagawa, Y.; Kawakami, T.; Yamanaka, S.; Yamaguchi, K.; Houk, K. N. *Mol. Phys.* **2002**, *100*, 717−727.
(13) Nicolaou, K. C.; Snyder, S. A.; Montagnon, T.; Vassilikogiannakis, G. *Angew. Chem., Int. Ed.* **2002**, *41*, 1668−1698.
(14) Corey, E. J. *Angew. Chem., Int. Ed.* **2002**, *41*, 1650−1667.
(15) Horn, B. A.; Herek, J. L.; Zewail, A. H. *J. Am. Chem. Soc.* **1996**, *118*, 8755−8756.
(16) Diau, E. W.-G.; De Feyter, S.; Zewail, A. H. *Chem. Phys. Lett.* **1999**, *304*, 134−144.
(17) Fuss, W.; Pushpa, K. K.; Schmid, W. E.; Trushin, S. A. *J. Phys. Chem A* **2001**, *105*, 10640−10645.
(18) Lewis, D. K.; Glenar, D. A.; Hughes, S.; Kalra, B. L.; Schlier, J.; Shukla, R.; Baldwin, J. E. *J. Am. Chem. Soc.* **2001**, *123*, 996−997.
(19) Beno, B. R.; Wilsey, S.; Houk, K. N. *J. Am. Chem. Soc*. **1999**, *121*, 4816−4826.
(20) Wilsey, S.; Houk, K. N.; Zewail, A. H. *J. Am. Chem. Soc.* **1999**, *121*, 5772−5786.
(21) Scacchi, G.; Richard, C.; Back, M. H. *Int. J. Chem. Kinet.* **1977**, *9*, 513−524.
(22) Scacchi, G.; Back, M. H. *Int. J. Chem. Kinet.* **1977**, *9*, 525−534.
(23) Gerberich, H. R.; Walters, W. D. *J. Am. Chem. Soc*. **1961**, *83*, 3935−3939.
(24) Pedersen, S.; Herek, J. L.; Zewail, A. H. *Science* **1994**, *266*, 1359−1364.
(25) De Feyter, S.; Diau, E. W.-G.; Scala, A. A.; Zewail, A. H. *Chem. Phys. Lett.* **1999**, *303*, 249−260.
(26) Bernardi, F.; Bottoni, A.; Olivucci, M.; Venturini, A.; Robb, M. A. *J. Chem. Soc., Faraday Trans.* **1994**, *90*, 1617−1630.
(27) Doubleday, C., Jr. *J. Am. Chem. Soc.* **1993**, *115*, 11968−11983.
(28) Doubleday, C., Jr. *J. Phys. Chem.* **1996**, *100*, 15083−15086.
(29) Moriarty, N. W.; Lindh, R.; Karlström, G. *Chem. Phys. Lett.* **1998**, *289*, 442−450.
(30) Vuilleumier, R.; Sprik, M. *Chem. Phys. Lett.* **2002**, *365*, 305−312.
(31) Huisgen, R. In *1,3-Dipolar cycloaddition chemistry*; Padwa, A., Ed.; Wiley: New York, 1984; Vol. 1, pp 47−70.
(32) Jónsson, H.; Mills G.; Jacobsen, K. W. In *Classical and Quantum Dynamics in Condensed Phase Simulations*; Berne, B. J., Ciccotti, G., Coker, D. F., Eds.; World Scientific: Singapore, 1998. Henkelman, G.; Jónsson, H. *J. Chem. Phys.* **2000**, *113*, 9978.
(33) E, W.; Ren, W. Q.; Vanden-Eijnden, E. *Phys. Rev. B* **2002**, *66*, 052301.
(34) *CPMD*, versions 3.5 and 3.4.1; Copyright IBM Corp: 1990−2001; Copyright MPI fuer Festkoerperforschung: Stuttgart, Germany, 1997−2001.
(35) Frisch, M. J.; Trucks, G. W.; Schlegel, H. B.; Scuseria, G. E.; Robb, M. A.; Cheeseman, J. R.; Zakrzewski, V. G.; Montgomery, J. A., Jr.; Stratmann, R. E.; Burant, J. C.; Dapprich, S.; Millam, J. M.; Daniels, A. D.; Kudin, K. N.; Strain, M. C.; Farkas, O.; Tomasi, J.; Barone, V.; Cossi, M.; Cammi, R.; Mennucci, B.; Pomelli, C.; Adamo, C.; Clifford, S.; Ochterski, J.; Petersson, G. A.; Ayala, P. Y.; Cui, Q.; Morokuma, K.; Malick, D. K.; Rabuck, A. D.; Raghavachari, K.; Foresman, J. B.; Cioslowski, J.; Ortiz, J. V.; Stefanov, B. B.; Liu, G.; Liashenko, A.; Piskorz, P.; Komaromi, I.; Gomperts, R.; Martin, R. L.; Fox, D. J.; Keith, T.; Al-Laham, M. A.; Peng, C. Y.; Nanayakkara, A.; Gonzalez, C.; Challacombe, M.; Gill, P. M. W.; Johnson, B. G.; Chen, W.; Wong, M. W.; Andres, J. L.; Head-Gordon, M.; Replogle, E. S.; Pople, J. A. *Gaussian 98*, revision A.11; Gaussian, Inc.: Pittsburgh, PA, 1998.
(36) Hohenberg, P.; Kohn, W. *Phys. Rev. B* **1964**, *136*, 864−871.
(37) Kohn, W.; Sham, L. J. *Phys. Rev. A* **1965**, *140*, 1133−1138.
(38) Jones, R. O.; Gunnarsson, O. *Rev. Mod. Phys.* **1989**, *61*, 689−746.
(39) Becke, A. D. *Phys. Rev. A* **1988**, *38*, 3098−3100.
(40) Lee, C.; Yang, W.; Parr, R. G. *Phys. Rev. B* **1988**, *37*, 785−789.
(41) Becke, A. D. *J. Chem. Phys.* **1993**, *98*, 5648−5652.
(42) Troullier, N.; Martins, J. L. *Phys. Rev. B* **1991**, *43*, 1993−2006.
(43) Goedecker, S.; Teter, M.; Hutter, J. *Phys. Rev. B* **1996**, *54*, 1703−1710.
(44) Boys, S. F. In *Quantum Theory of Atoms, Molecules, and the Solid State*; Löwdin, P.-O., Ed.; Academic Press: New York, 1966; pp 253−262.
(45) Silvestrelli, P. L.; Marzari, N.; Vanderbilt, D.; Parrinello, M. *Solid State Commun.* **1998**, *107*, 7−11.
(46) Berghold, G.; Mundy, C. J.; Romero, A. H.; Hutter, J.; Parrinello, M. *Phys. Rev. B* **2000**, *61*, 10040−10048.
(47) Silvestrelli, P. L. *Phys. Rev. B* **1999**, *59*, 9703−9706.
(48) Resta, R. *Phys. Rev. Lett.* **1998**, *80*, 1800−1803.
(49) Holleman, A. F.; Wiberg, N. *Lehrbuch der Anorganischen Chemie*; Walter de Gruyter: Berlin, 1995; pp 1838−1841.
(50) Aktah, D.; Frank, I. *J. Am. Chem. Soc*. **2002**, *124*, 3402−3406.
(51) Boero, M.; Parrinello, M.; Hüffer, S.; Weiss, H. *J. Am. Chem. Soc.* **2000**, *122*, 501−509.
(52) Mundy, C. J.; Hutter, J.; Parrinello, M. *J. Am. Chem. Soc.* **2000**, *122*, 4837−4838.
(53) The influence of explicit Hartree−Fock exchange in the form of the hybrid density functional B3LYP and the effect of dynamic correlation (Møller−Plesset perturbation theory) on this energy difference is shown. In the latter, two types of calculations can be distinguished: one in which all of the orbitals (FULL) are included in the correlation calculation and a second one in which the inner shells are excluded from the correlation calculation ("frozen-core" = FC).
(54) Tanaka, S.; Chernyak, V.; Mukamel, S. *Phys. Rev. A* **2001**, *63*, 063405-1−063405-14.
(55) Tanaka, S.; Mukamel, S. *Phys. Rev. A* **2001**, *64*, 032503-1−032503-13.